

High-throughput imaging measurements of thermoelectric figure of merit

Abdulkareem Alasli^{a,*}, Asuka Miura^{b,*†}, Ryo Iguchi^b, Hosei Nagano^a and Ken-ichi Uchida^{b,c,d}

^aDepartment of Mechanical Systems Engineering, Nagoya University, Nagoya 464-8601, Japan;

^bNational Institute for Materials Science, Tsukuba 305-0047, Japan;

^cInstitute for Materials Research, Tohoku University, Sendai 980-8577, Japan;

^dCenter for Spintronics Research Network, Tohoku University, Sendai 980-8577, Japan

*These authors contributed equally to this work.

†Present address: Integrated Research for Energy and Environment Advanced Technology, Kyushu Institute of Technology, Kitakyushu, Fukuoka 804-8550, Japan

CONTACT Ken-ichi Uchida UCHIDA.Kenichi@nims.go.jp

We demonstrate a method for the simultaneous determination of the thermoelectric figure of merit of multiple materials by means of the lock-in thermography (LIT) technique. This method is based on the thermal analyses of the transient temperature distribution induced by the Peltier effect and Joule heating, which enables high-throughput estimation of the thermal diffusivity, thermal conductivity, volumetric heat capacity, Seebeck or Peltier coefficient of the materials. The LIT-based approach has high reproducibility and reliability because it offers sensitive noncontact temperature measurements and does not require the installation of an external heater. By performing the same measurements and analyses with applying an external magnetic field, the magnetic field and/or magnetization dependences of the Seebeck or Peltier coefficient and thermal conductivity can be determined simultaneously. We demonstrate the validity of this method by using several ferromagnetic metals (Ni, Ni₉₅Pt₅, and Fe) and a nonmagnetic metal (Ti). The proposed method will be useful for materials research in thermoelectrics and spin caloritronics and for investigation of magneto-thermal and magneto-thermoelectric transport properties.

Keywords: Thermoelectric effects; figure of merit; thermopower; thermal conductivity; lock-in thermography; magnetic materials; spin caloritronics

1. Introduction

The Seebeck and Peltier effects refer to the conversion of heat into electricity and vice versa [1–3]. Since the discovery of these fundamental thermoelectric phenomena, many developments in physics, materials science, and applications have been achieved in order to fulfill the increasing global demands for energy [4–6]. In this context, accurate evaluation of the performance of thermoelectric materials is of great importance. The dimensionless figure of merit ZT is a well-known parameter representing the performance of thermoelectric materials [7]. ZT can be measured directly or derived from the transport properties of a material since it is defined as

$$ZT = \frac{S^2 \sigma}{\kappa} T \left(= \frac{\Pi^2 \sigma}{\kappa} \frac{1}{T} \right), \quad (1)$$

where $S = \Pi/T$, σ , κ , and T are the Seebeck coefficient with Π being the Peltier coefficient, electrical conductivity, thermal conductivity, and absolute temperature, respectively [3]. The direct measurement of ZT is realized by the so-called Harman method, which determines ZT from the voltage responses of a material to DC and AC charge currents with a single apparatus [8,9]. The accuracy of the Harman method, however, can be affected by unavoidable electrical contact resistance and heat leakage through measurement probes [10]. Therefore, ZT is often estimated by measuring S , σ , and κ independently, although such

measurements require a wide range of time-consuming experiments and lead to larger combined uncertainties [11].

In this article, we propose a different approach for determining ZT based on the lock-in thermography (LIT). LIT is an active thermal imaging technique that allows the detection of the thermal response in a sample to a periodic external perturbation with high temperature resolution [12]. Although LIT was originally developed for nondestructive testing of electronic components [13], it has shown notable performance in the measurements of various properties including the Peltier coefficient [14], thermal diffusivity [15], magnetocaloric effects [16,17], magneto-thermoelectric effects [18–22], and thermo-spin effects [23,24]. Here, we show that LIT also enables simultaneous measurements of S and κ , allowing the rapid derivation of ZT with a single apparatus. Since LIT is a noncontact thermal imaging technique, the thermoelectric and thermal transport properties of multiple materials can be measured at the same time without the disturbance of heat leakage through temperature probes. The proposed method can be easily extended to the measurements under magnetic fields, enabling the investigation of magneto-thermal resistance [22] and magneto-thermoelectric effects.

2. Measurement and analysis procedures

The basic concept and principle of the LIT-based ZT measurement method are illustrated in Figure 1. The setup consists of an infrared camera connected to a processing system and current source. A typical sample is a bar-shaped junction comprising thermoelectric and reference materials [Figure 1(a)]. The estimation of S and κ of the thermoelectric material is the target of this measurement, while the transport properties of the reference material are given parameters. When a charge current \mathbf{J}_c is applied to the junction, the temperature change due to the Peltier effect (Joule heating) appears at the junction interface (in the bulk of the materials). LIT enables the imaging of the transient temperature modulation signals induced by the Peltier effect and Joule heating and the separation of them as follows. Under a square-wave-modulated AC charge current with the frequency f , amplitude J_c , and zero DC offset, an oscillating heat release and absorption due to the Peltier effect with the same f and a constant heat release due to the Joule heating are induced [LIT measurement 1 in Figure 1(b)]. On the other hand, under a current with the frequency f , amplitude $J_c/2$, and DC offset $J_c/2$, oscillating Peltier and Joule-heating signals with the same f are induced [LIT measurement 2 in Figure 1(c)]. Consequently, in the LIT measurement 1, LIT outputs the lock-in amplitude A_Π and phase ϕ_Π images of the Peltier-effect-induced temperature modulation through Fourier analysis [12], where the Joule-heating contribution is eliminated by extracting the first harmonic response of the temperature modulation. Here, the amplitude image shows the spatial distribution of the magnitude of the temperature modulation, while the phase image shows the time delay of the temperature modulation and heat flux direction. In contrast, in the LIT measurement 2, both the Peltier and Joule-heating contributions appear in LIT images. Thus, to extract the amplitude A_J and phase ϕ_J images of the Joule-heating-induced temperature modulation, we subtract the half of the Peltier-effect-induced LIT signals obtained in the LIT measurement 1 from raw LIT signals in the LIT measurement 2, which cancels the Peltier contribution because of the absence of the Joule-heating contribution in the LIT measurement 1. Based on the thermal analyses of the obtained images, the parameters of interest can be obtained, as detailed below.

Figure 1(d) summarizes the modelling and sequence of the thermal analyses in our method. During the LIT measurements, the Peltier effect generates an oscillating heat current density $\mathbf{q} = \Pi \mathbf{j}_c$ in the thermoelectric and reference materials, where \mathbf{j}_c is a current charge density. At the junction, \mathbf{q} becomes discontinuous due to the difference in Π between the thermoelectric and reference materials, which leads to finite heating or cooling $Q_\Pi (= -\nabla \cdot \mathbf{q})$. The oscillating Q_Π in time diffuses as heat waves from the junction into each material. The propagation of the heat waves is dominated by the thermal diffusivity $D = \kappa/(\rho c_p)$ with ρ and c_p respectively being the density and specific heat capacity. Due to the difference in the thermophysical properties, Q_Π diffuses asymmetrically and the induced temperature modulation ΔT_Π decays exponentially along the bar [Figure 1(d)]. The ΔT_Π distribution in each material can be obtained by solving the one-dimensional heat equation along the x direction for the infinitely long junction system, whose interface is located at $x = 0$ and the thermoelectric (reference) material spans $x < 0$ ($x > 0$) [25]. ΔT_Π is assumed to be continuous at the interface by neglecting the interfacial thermal resistance and to be zero at the system boundaries ($x \rightarrow \pm\infty$). Under the adiabatic condition, the amplitude $A_\Pi^{\text{TE(Ref)}}$ and phase delay $\phi_\Pi^{\text{TE(Ref)}}$ of the first harmonic of the steady periodic solution of ΔT_Π is given by

$$A_{\Pi}^{\text{TE(Ref)}}(x) = \sqrt{\frac{8}{\pi^3 f}} \frac{(\Pi_{\text{TE}} - \Pi_{\text{Ref}}) j_c}{(\kappa_{\text{Ref}} / \sqrt{D_{\text{Ref}}} + \kappa_{\text{TE}} / \sqrt{D_{\text{TE}}})} e^{+(-)\sqrt{\frac{D_{\text{TE(Ref)}}}{\pi f}} x}, \quad (2)$$

$$\phi_{\Pi}^{\text{TE(Ref)}}(x) = -(+)\sqrt{\frac{D_{\text{TE(Ref)}}}{\pi f}} x + \frac{\pi}{4}, \quad (3)$$

where j_c denotes the square-wave amplitude of the charge current density and the superscripts or subscripts TE and Ref refer to the thermoelectric and reference materials, respectively. Similarly, the Joule-heating-induced temperature modulation ΔT_J can be obtained by solving the heat balance equation under the condition of negligible heat losses [26,27]; the amplitude $A_J^{\text{TE(Ref)}}$ and phase delay ϕ_J of ΔT_J are given by

$$A_J^{\text{TE(Ref)}} = \frac{D_{\text{TE(Ref)}} j_c^2}{\pi^2 f \sigma_{\text{TE(Ref)}} \kappa_{\text{TE(Ref)}}}, \quad (4)$$

$$\phi_J = \frac{\pi}{2} \quad (5)$$

Here, the heat release or absorption due to the temperature dependence of S , i.e., the Thomson effect, is neglected because its contribution in metals is usually small [28,29]. Accordingly, by analyzing the LIT images using Equations (2)-(4), D , κ , Π , and ZT of the thermoelectric material can be determined [Figure 1(d)]. D can be derived by fitting observed A_{Π} profiles with Equation (2) (referred to as D_A) and ϕ_{Π} profiles with Equation (3) (referred to as D_{ϕ}). κ can be then determined from A_J by using the σ values measured separately. Subsequently, Π and S can be calculated from A_{Π} with respect to the reference material. ZT is then estimated based on Equation (1).

To demonstrate the usability of the proposed method, we measured the thermal responses from four different materials simultaneously by means of LIT. We used polycrystalline Ni, Ni₉₅Pt₅, Fe, and Ti slabs as thermoelectric materials and a Cu slab as a reference material. The Ni, Fe, Ti, and Cu slabs are commercially available from the Nilaco Corporation, Japan, and the Ni₉₅Pt₅ slab, prepared by a melting method with rapid cooling, is available from Kojundo Chemical Laboratory Co., Ltd., Japan. The Ni/Cu, Ni₉₅Pt₅/Cu, Fe/Cu, and Ti/Cu junctions were prepared by a spark plasma sintering method at 800 °C under a pressure of 30 MPa for 5 minutes in a vacuum. The junctions were then cut into a bar shape with a width of 0.6 mm, thickness of 0.5 mm, and total length of 24.0 mm, where the length of each material is 12.0 mm. For the LIT measurements, the junctions were arranged in parallel with a gap of ~0.8 mm in the focal plane of the infrared camera, electrically connected in series, and suspended in air to prevent heat loss [Figure 1(a)]. To unify and enhance the infrared emission, the top surfaces of the junctions were coated with an insulating black ink with the infrared emissivity of >0.94. The calibration process to convert the observed infrared radiation intensity into temperature is detailed in [19]. The LIT measurements were performed while applying J_c with a square-wave amplitude of 1 A and frequency of $f = 0.5$ -12.5 Hz to the junctions at room temperature, where the direction of J_c was fixed in all the junctions [Figure 1(a)]. We also measured D , κ , S , and σ of the materials by conventional methods (Table 1); the σ values of all the materials and the parameters of Cu were used for the LIT-based thermal analyses, while the remaining parameters were used for the comparison to confirm the validity of the proposed method.

3. Results and discussion

Figure 2 shows the A_{Π} , ϕ_{Π} , A_J , and ϕ_J images and corresponding line profiles averaged over the center area of the samples at $f = 10$ Hz, where the target materials (Ni, Ni₉₅Pt₅, Fe, and Ti) and the reference material (Cu) are on the left and right halves, respectively. In the LIT measurement 1, clear current-induced temperature modulation signals appear in the vicinity of the junctions [A_{Π} and ϕ_{Π} images in Figures 2(a) and 2(b)]. As shown in the line profiles, the A_{Π} (ϕ_{Π}) values exhibit asymmetrical exponential decay (linear change) with respect to the distance from the junctions. These behaviors are consistent with Equations (2) and (3), indicating that the signals in the A_{Π} and ϕ_{Π} images originate from the oscillating Q_{Π} at the junctions. The continuity of A_{Π} and ϕ_{Π} at the junctions ensures that the interfacial thermal resistance is negligibly small. Importantly, the ϕ_{Π} values at the Ni/Cu and Ni₉₅Pt₅/Cu junctions differ by 180° from those at the Fe/Cu and Ti/Cu junctions, indicating that the sign of the temperature modulation for the former junctions

is opposite to that for the latter junctions. This result is consistent with the fact that the relative Peltier coefficients for the Ni/Cu and Ni₉₅Pt₅/Cu junctions are opposite in sign to those for the Fe/Cu and Ti/Cu junctions (Table 1). The weak A_{Π} decay and small ϕ_{Π} slope in Cu can be explained by the large D of Cu. Qualitatively similar results were obtained at various values of f (Figure S1 in the supplementary material). On the other hand, in the A_J and ϕ_J images, almost uniform temperature modulation signals appear in the bulk of the materials; no signals at the junctions confirm that the Joule-heating contribution is extracted without the contamination by the Peltier contribution. As shown in Figure 2(c), the largest (smallest) Joule-heating signals were observed in Ti (Cu), consistent with Equation (4) and the parameters in Table 1. It is worth mentioning that the non-uniformity of A_J and ϕ_J can be seen near the junctions due to the heat leakage between the materials. Such artifacts are suppressed with increasing f (Figure S2 in the supplementary material). Thus, the accuracy of the LIT-based thermal analyses is improved at higher f . We also confirmed that, when $f > 5$ Hz, the heat loss at both the ends of the samples as well as the natural convection and thermal radiation are negligible in the LIT images (see the supplementary material).

Figures 3(a)-3(d) respectively show the f dependence of D , κ , S (Π), and ZT at $T = 300$ K for the target materials, obtained by analyzing the LIT images. The obtained D_A and D_{ϕ} values show notable deviation at low f because of the heat loss [the inset to Figure 3(a)]. The heat loss effects can be minimized by taking the geometric mean $D = \sqrt{D_A D_{\phi}}$ [30], which is almost independent of f and in good agreement with the values measured by the conventional method [Figure 3(a)]. The κ values obtained by substituting A_J^{TE} , D , and σ into Equation (4) are shown in Figure 3(b); although the heat loss effects are unavoidable at low f , the results for $f > 5$ Hz are consistent with the values in Table 1 and the literature [19,31–33]. Figures 3(c) and 3(d) show S (and the corresponding Π) and ZT at $T = 300$ K for the materials, respectively. The consistency of the magnitude and sign of the coefficients confirms that the LIT-based method enables simultaneous estimation of thermal and thermoelectric properties. We also note that the ρc_p values estimated from the LIT-based analyses are also consistent with the values measured by the conventional methods (Figure S3 in the supplementary material).

To confirm the versatility of the LIT-based method, we performed the same measurements and thermal analyses with applying a magnetic field \mathbf{H} (with the magnitude H) to the samples. Although the H dependence of the electron transport coefficients is small in typical metals, σ , κ , and S (Π) of ferromagnetic metals depend on the magnetization direction due to the anisotropic magnetoresistance, anisotropic magneto-thermal resistance, and anisotropic magneto-Seebeck (Peltier) effects, respectively [22]. Here, we show that the LIT-based method can be used for the simultaneous measurements of the anisotropic magneto-thermal resistance and anisotropic magneto-Seebeck and Peltier effects for many materials. We took the anisotropic magnetoresistance, i.e., the H dependence of σ , into account in the following analyses but found that its contribution is negligibly small. In the experiments, the uniform \mathbf{H} was applied along the longitudinal direction of the samples by using an electromagnet. The highest intensity of \mathbf{H} is $\mu_0 H = 150$ mT with μ_0 being the vacuum permeability, which is large enough to saturate the magnetization of all the bar-shaped ferromagnets [21].

Figure 4(a) shows the H dependence of S , obtained from the LIT-based method. The small but finite H dependence of S was observed to appear in Ni and Ni₉₅Pt₅, while no clear dependence was observed in Fe and Ti. The H -dependent change ratio of S for Ni₉₅Pt₅ is larger than that for Ni [Figure 4(d)], consistent with the previous report on the anisotropic magneto-Seebeck and Peltier effects [19,21]. We also found that the H dependence of κ for Ni and Ni₉₅Pt₅ is larger than that for Fe and Ti [Figures 4(b) and 4(e)]. The resultant H dependence of ZT calculated based on Equation (1) is shown in Figures 4(c) and 4(f). Ni₉₅Pt₅ exhibits the largest ZT change, while Fe and Ti show almost no H dependence; the observed H -dependent change ratio of ZT at $\mu_0 H = 150$ mT are -10.5% , -16.8% , 1.5% , and -0.4% for Ni, Ni₉₅Pt₅, Fe, and Ti, respectively [Figure 4(f)]. In the materials used in this study, the magnetic field or magnetization dependent effects do not contribute to the enhancement of the thermoelectric performance. Nevertheless, the LIT-based method is useful because it enables simultaneous measurements of the H dependence of S and κ for many samples.

Finally, we discuss the applicability limit of the LIT-based ZT measurement method. The same LIT measurements and thermal analyses are applicable not only to metals but also to semiconductors when the interfaces comprising thermoelectric and reference materials exhibit Ohmic contact and negligible interfacial thermal resistance. In contrast, if a sample has large interfacial thermal resistance and exhibits discontinuous temperature modulation at the interface, the same analyses are not valid. The generalization of the LIT-based method to a system with finite interfacial thermal resistance is a remaining task for future studies.

4. Conclusion

We have proposed and demonstrated a ZT measurement method via the noncontact thermal imaging based on LIT. In this method, D , κ , S (Π), and ZT of multiple materials can be simultaneously estimated from the thermal analyses of the transient temperature distributions induced by the Peltier effect and Joule heating, enabling systematic, high-throughput, and versatile investigations of the thermal and thermoelectric properties. The parameters obtained by the LIT-based method are consistent with the values obtained by the conventional methods. This method can also be used for investigating the magnetic field or magnetization dependence of the thermal and thermoelectric transport properties. Although we measured the electrical conductivity separately from LIT, it is easy to integrate four-probe electrical measurements into a LIT system; by using such an integrated system, all the transport properties associated with ZT can be measured with a single apparatus. Thus, we anticipate that the LIT-based ZT measurement method will accelerate materials science research in thermoelectrics as well as spin caloritronics [22,34,35].

Acknowledgments

The authors thank H. Ohta and T. Yamazaki for valuable discussions.

Disclosure statement

The authors have no conflicts of interest directly relevant to the content of this article.

Data availability statement

The data that support the findings of this study are available from the corresponding author upon reasonable request.

Funding

This work was supported by CREST “Creation of Innovative Core Technologies for Nano-enabled Thermal Management” (JPMJCR17I1) from JST, Japan. A.M. was supported by JSPS through Research Fellowship for Young Scientists (18J02115).

References

- [1] Seebeck TJ. Ueber die magnetische polarisation der metalle und erze durch temperaturdifferenz. Abh Dtsch Akad Wiss Berlin. 1823;265:1822.
- [2] Peltier JCA. Nouvelle experiences sur la caloricit  des courants  lectriques. Ann Chim Phys. 1834;56:371.
- [3] Rowe DM. CRC Handbook of thermoelectrics. Rowe DM, editor. CRC Press; 1995.
- [4] Dresselhaus MS, Chen G, Tang MY, et al. New directions for low-dimensional thermoelectric materials. Adv Mater. 2007;19:1043–1053.
- [5] Cui J, Gao Y, Zhou H, et al. Significantly enhanced thermoelectric figure of merit through Cu, Sb co-substitutions for Te in Ga₂Te₃. Appl Phys Lett. 2012;101:081908.
- [6] He J, Tritt TM. Advances in thermoelectric materials research: Looking back and moving forward. Science. 2017;357:eaak9997.
- [7] Narducci D. Do we really need high thermoelectric figures of merit? A critical appraisal to the power conversion efficiency of thermoelectric materials. Appl Phys Lett. 2011;99:102104.
- [8] Harman TC. Special techniques for measurement of thermoelectric properties. J Appl Phys. 1958;29:1373–1374.
- [9] Roh I-J, Lee YG, Kang M-S, et al. Harman measurements for thermoelectric materials and modules under non-adiabatic conditions. Sci Rep. 2016;6:39131.
- [10] Kang M-S, Roh I-J, Lee YG, et al. Correction of the electrical and thermal extrinsic effects in thermoelectric measurements by the Harman method. Sci Rep. 2016;6:26507.

- [11] Borup KA, de Boor J, Wang H, et al. Measuring thermoelectric transport properties of materials. *Energy Environ Sci.* 2015;8:423–435.
- [12] Breitenstein O, Warta W, Langenkamp M. Lock-in thermography: Basics and use for evaluating electronic devices and materials. Berlin/Heidelberg, Germany: Springer; 2010.
- [13] Kuo PK, Ahmed T, Jin H, et al. Phase-locked image acquisition in thermography. In: Chen MJW, editor. Automated inspection high-speed vision architecture II. SPIE; 1989. p. 41.
- [14] Straube H, Wagner J-M, Breitenstein O. Measurement of the Peltier coefficient of semiconductors by lock-in thermography. *Appl Phys Lett.* 2009;95:52107.
- [15] Ishizaki T, Nagano H. Measurement of 3D thermal diffusivity distribution with lock-in thermography and application for high thermal conductivity CFRPs. *Infrared Phys Technol.* 2019;99:248–256.
- [16] Hirayama Y, Iguchi R, Miao X-F, et al. High-throughput direct measurement of magnetocaloric effect based on lock-in thermography technique. *Appl Phys Lett.* 2017;111:163901.
- [17] Modak R, Iguchi R, Sepehri-Amin H, et al. Simultaneous direct measurements of conventional and inverse magnetocaloric effects in Ni–Mn-based Heusler alloys using lock-in thermography technique. *AIP Adv.* 2020;10:065005.
- [18] Seki T, Iguchi R, Takanashi K, et al. Visualization of anomalous Ettingshausen effect in a ferromagnetic film: Direct evidence of different symmetry from spin Peltier effect. *Appl Phys Lett.* 2018;112:152403.
- [19] Uchida K, Daimon S, Iguchi R, et al. Observation of anisotropic magneto-Peltier effect in nickel. *Nature.* 2018;558:95–99.
- [20] Miura A, Sepehri-Amin H, Masuda K, et al. Observation of anomalous Ettingshausen effect and large transverse thermoelectric conductivity in permanent magnets. *Appl Phys Lett.* 2019;115:222403.
- [21] Miura A, Iguchi R, Seki T, et al. Spin-mediated charge-to-heat current conversion phenomena in ferromagnetic binary alloys. *Phys Rev Mater.* 2020;4:034409.
- [22] Uchida K. Transport phenomena in spin caloritronics. *Proc Japan Acad Ser B.* 2021;97:69–88.
- [23] Wid O, Bauer J, Müller A, et al. Investigation of the unidirectional spin heat conveyer effect in a 200 nm thin Yttrium Iron Garnet film. *Sci Rep.* 2016;6:28233.
- [24] Daimon S, Iguchi R, Hioki T, et al. Thermal imaging of spin Peltier effect. *Nat Commun.* 2016;7:13754.
- [25] Carslaw HS, Jaeger JC. Conduction of heat in solids. Clarendon press; 1992.
- [26] Sullivan PF, Seidel G. Steady-state, AC-temperature calorimetry. *Phys Rev.* 1968;173:679–685.
- [27] Baloga JD, Garland CW. AC calorimetry at high pressure. *Rev Sci Instrum.* 1977;48:105–110.
- [28] Thomson W. 4. On a Mechanical theory of thermo-electric currents. *Proc R Soc Edinburgh.* 1851;3:91–98.
- [29] Uchida K, Murata M, Miura A, et al. Observation of the magneto-Thomson effect. *Phys Rev Lett.* 2020;125:106601.
- [30] Gu Y, Tang X, Xu Y, et al. Ingenious method for eliminating effects of heat loss in measurements of thermal diffusivity by ac calorimetric method. *Jpn J Appl Phys.* 1993;32:L1365–L1367.
- [31] Powell RW, Tye RP, Hickman MJ. The thermal conductivity of nickel. *Int J Heat Mass Transf.* 1965;8:679–688.
- [32] Ho CY, Powell RW, Liley PE. Thermal conductivity of the elements. *J Phys Chem Ref Data.* 1972;1:279–421.
- [33] Haynes WM. CRC handbook of chemistry and physics. Haynes WM, editor. CRC press; 2014.
- [34] Bauer GEW, Saitoh E, van Wees BJ. Spin caloritronics. *Nat Mater.* 2012;11:391–399.
- [35] Boona SR, Myers RC, Heremans JP. Spin caloritronics. *Energy Environ Sci.* 2014;7:885.

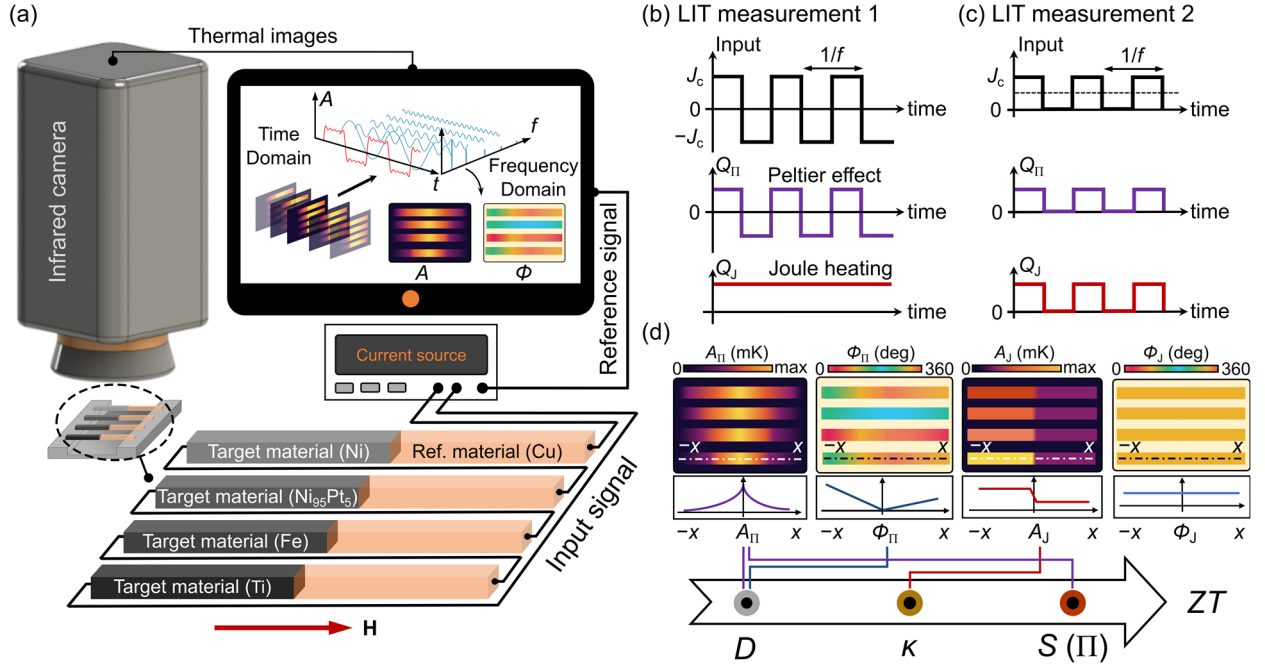


Figure 1. (a) Schematic of the LIT-based ZT measurement technique. The samples are the bar-shaped junctions consisting of a thermoelectric material (target material; Ni, Ni₉₅Pt₅, Fe, and Ti) and a reference material (Cu). H denotes the external magnetic field. (b), (c) LIT conditions for measuring the temperature distribution induced by the Peltier effect (LIT measurement 1) and by the Joule heating (LIT measurement 2). In the LIT measurement 1 (2), a square-wave AC current with the frequency f , amplitude J_c ($J_c/2$), and zero offset (finite DC offset $J_c/2$) is applied to the junctions. Q_{Π} (Q_J) denotes heat release or absorption due to the Peltier effect (heat release due to the Joule heating). (d) Sequence of obtaining the thermal diffusivity D , thermal conductivity κ , Seebeck coefficient S (Peltier coefficient Π), and ZT by thermal analyses of LIT images. A_{Π} and ϕ_{Π} (A_J and ϕ_J) denote the lock-in amplitude and phase of the temperature modulation induced by the Peltier effect (Joule heating), respectively.

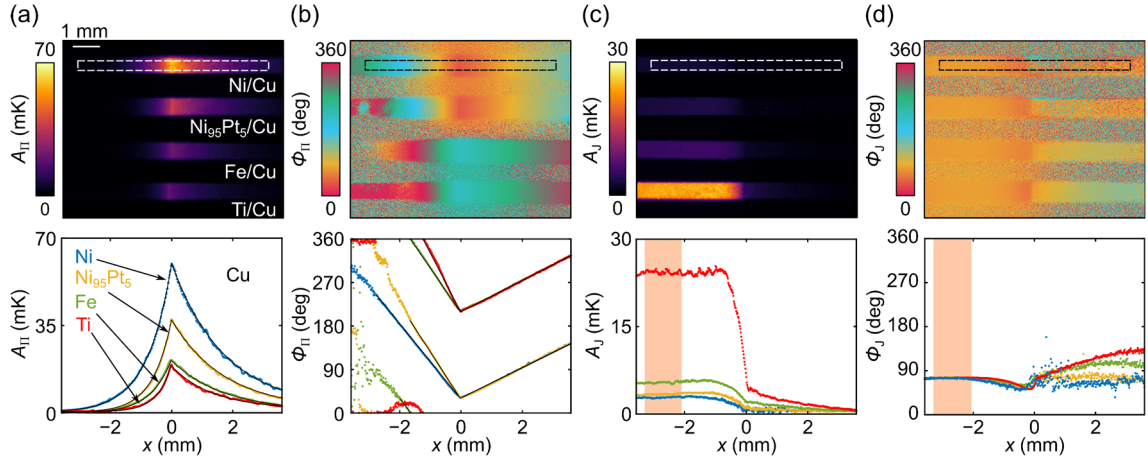


Figure 2. (a) A_{Π} , (b) ϕ_{Π} , (c) A_J , and (d) ϕ_J images and corresponding line profiles along the longitudinal direction (x direction) for the Ni/Cu, Ni₉₅Pt₅/Cu, Fe/Cu, and Ti/Cu samples at $f = 10$ Hz and $J_c = 1$ A. In each image, the junctions are placed around the center; the left (right) half in the images and line profiles corresponds to the target materials (reference material). The line profiles were obtained by taking the average of the raw profiles over the center areas (dashed rectangles) of the samples. $x = 0$ in the line profiles was determined by the peak position of A_{Π} for each sample. The solid black lines in (a) and (b) represent the fitting results using Equations (2) and (3), respectively. The LIT data shown in this figure were measured in the absence of an external magnetic field.

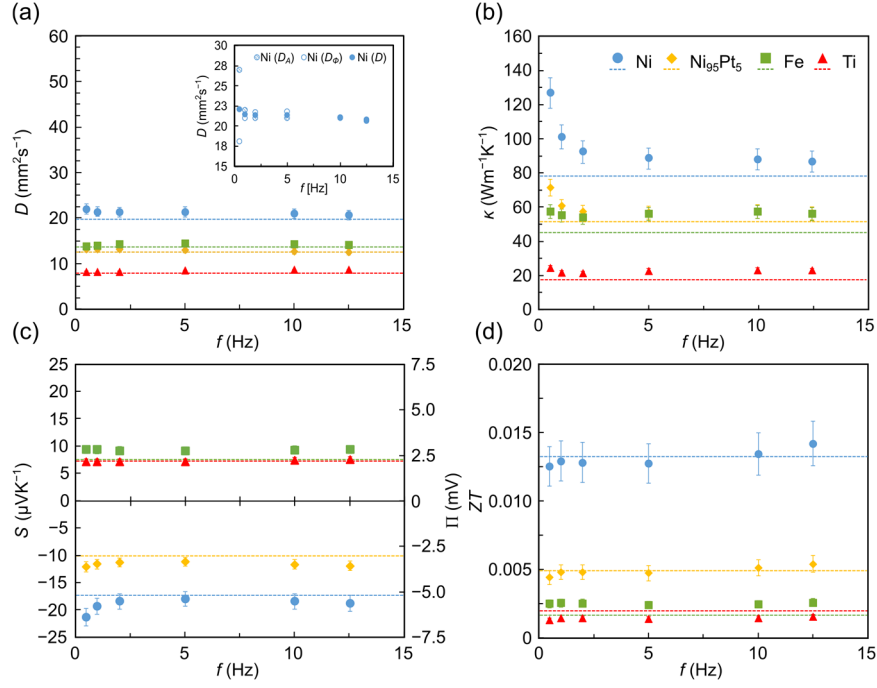


Figure 3. f dependence of (a) D , (b) κ , (c) S (and the corresponding Π), and (d) ZT at $T = 300$ K for the Ni (blue circle), $\text{Ni}_{95}\text{Pt}_5$ (yellow diamond), Fe (green square), and Ti (red triangle) samples. D was obtained from the geometric mean $D = \sqrt{D_A D_\phi}$ with the thermal diffusivity D_A obtained from the A_Π image and D_ϕ obtained from the ϕ_Π image by fitting. To estimate κ , we averaged the A_j values over the orange rectangle areas in Figure 2, where the slope of the Joule-heating signal is negligibly small for $f > 5$ Hz (Figure S2 in the supplementary material). The dashed lines represent the values obtained by the conventional methods, where D was measured by the laser flash method, κ was estimated from D , specific heat capacity measured by the differential scanning calorimetry, and density measured by the Archimedes method, and S and σ were measured by using Seebeck Coefficient/Electric Resistance Measurement System (ZEM-3, ADVANCE RIKO, Inc.).

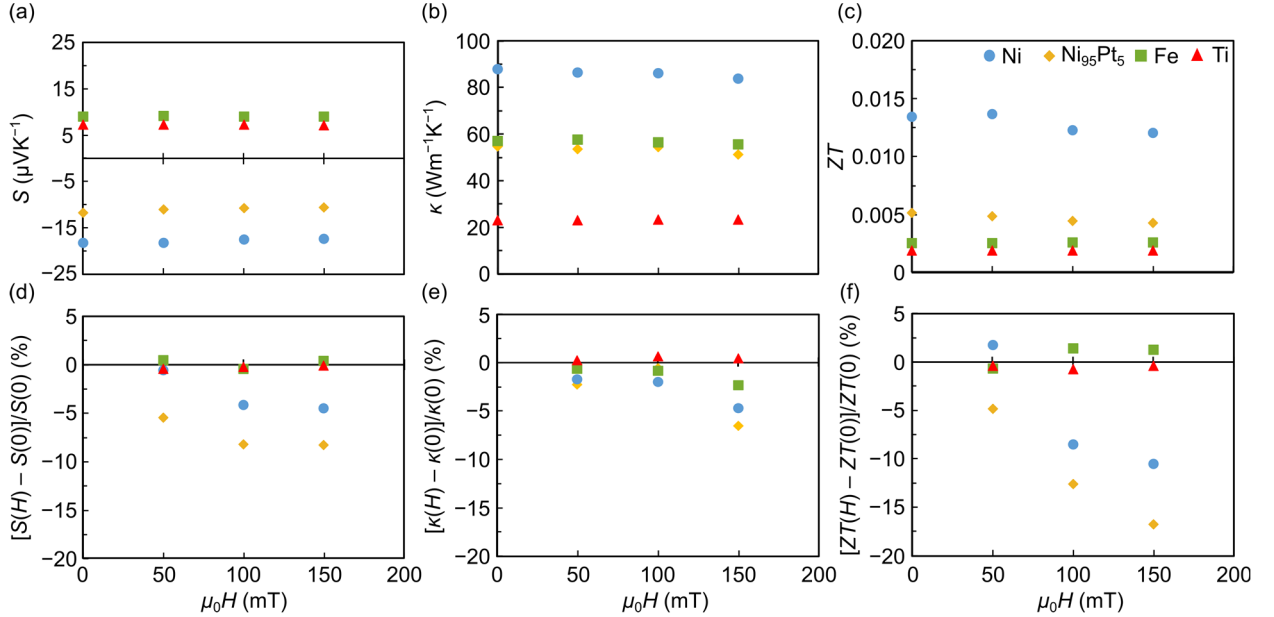


Figure 4. (a)-(c) H dependence of S , κ , and ZT at $T = 300$ K for the Ni (blue circle), $\text{Ni}_{95}\text{Pt}_5$ (yellow diamond), Fe (green square), and Ti (red triangle) samples. (d)-(f) H dependence of $[S(H) - S(0)]/S(0)$, $[\kappa(H) - \kappa(0)]/\kappa(0)$, and $[ZT(H) - ZT(0)]/ZT(0)$. $S(0)$, $\kappa(0)$, and $ZT(0)$ denote the parameters at $\mu_0 H = 0$ mT with μ_0 being the vacuum permeability. The data shown in this figure were estimated from the LIT images at $f = 10$ Hz.

Table 1. D , κ , S , and σ of the materials measured by the conventional methods in the absence of a magnetic field.

Material	D (mm ² s ⁻¹)	κ (Wm ⁻¹ K ⁻¹)	S (μ VK ⁻¹)	σ (Sm ⁻¹)
Cu	123.2	425.1	2.5	57.8×10^6
Ni	19.8	78.1	-17.2	11.7×10^6
Ni ₉₅ Pt ₅	12.6	44.9	-10.1	7.2×10^6
Fe	13.7	51.4	7.4	5.3×10^6
Ti	7.9	17.6	7.6	2.0×10^6

Supplementary material

S1. Lock-in frequency dependence of temperature modulation and heat loss

Figure S1 shows the A_{Π} and ϕ_{Π} images and corresponding line profiles for various values of f for the Ni/Cu, Ni₉₅Pt₅/Cu, Fe/Cu, and Ti/Cu samples at $\mu_0 H = 0$ mT. The clear temperature modulation induced by the Peltier effect appears at all the f values but its spatial distribution depends on f . Because the temperature broadening due to thermal diffusion is suppressed by increasing f , the temperature modulation at higher f values exhibits a sharper peak around the junctions. The f -dependent temperature broadening is characterized by the thermal diffusion length $\Lambda = [D/(\pi f)]^{0.5}$. Thus, the effect of the heat leakage at the ends of the samples can be reduced by increasing f , as discussed in the main text. In contrast, the magnitude of the temperature modulation monotonically decreases with increasing f ; when the Peltier coefficient of a target material is small, one may have to decrease f to improve the signal-to-noise ratio. The f value should be determined by balancing these two factors.

The f dependence of the temperature modulation induced by Joule heating is shown in Figure S2. The appropriate f value for the LIT-based thermal analyses can be determined in a similar manner to the case of the temperature modulation induced by the Peltier effect.

Here, we discuss the effects of heat loss on the accuracy of the measurements. In general, heat transfer from the samples occurs via the thermal radiation Q_{rad} , convection Q_{conv} , and conduction Q_{cond} [1,2]. Because of the small temperature modulation observed in this study, the effect of Q_{rad} and Q_{conv} can be estimated via $Q_{\text{rad}} + Q_{\text{conv}} \propto h(T - T_{\text{amb}})$, where $h = h_{\text{rad}} + h_{\text{conv}}$ is the combined heat transfer coefficient, T the sample temperature, and T_{amb} the ambient temperature [1,3]. At these conditions, $h_{\text{rad}} = 4\varepsilon\delta T_{\text{amb}}^3$ gives a maximum value of $\sim 6 \text{ Wm}^{-2}\text{K}^{-1}$ for the extreme case of a blackbody (emissivity $\varepsilon = 1$), where δ is the Stefan-Boltzmann constant. On the other hand, h_{conv} at lowest f shown in Figure S2 is estimated to be $\sim 3 \text{ Wm}^{-2}\text{K}^{-1}$ for a horizontal slab [4], resulting in the total h of $\sim 9 \text{ Wm}^{-2}\text{K}^{-1}$. In the measurements of the Peltier effect, the heat loss ratio can be evaluated by $(Q_{\text{rad}} + Q_{\text{conv}})/Q_{\Pi} \sim (h/\kappa d)\Lambda^2$, where κ and d are the thermal conductivity and thickness of the slab, respectively [3]. On the other hand, the heat loss ratio in the measurements of Joule heating can be evaluated by $(Q_{\text{rad}} + Q_{\text{conv}})/Q_J \sim h/(\rho_p d)$. Based on these assumptions and the parameters measured by the conventional method (Table 1), we confirmed that the heat loss ratios are always less than 1% in the measurement f range. The heat loss due to Q_{cond} in our experimental setup represents the heat leaked from both the ends of the samples to the reference material and the electrical connection since the samples are suspended in air. In the measurements of the Peltier effect, the Q_{cond} contribution can be neglected if Λ is shorter than the distance between the junction and the region of interest, which can be controlled by changing f [3]. In the same manner, the effect of Q_{cond} on the Joule heating measurements can be neglected at high f . By using the D values in Table 1, we estimated Λ at $f = 5$ Hz to be 1.1, 0.9, 0.9, and 0.7 mm for Ni, Ni₉₅Pt₅, Fe, and Ti, respectively, much less than the length of the sample. This estimation confirms that the LIT-based thermal analyses are not affected by Q_{cond} for $f > 5$ Hz. Thus, we selected the data at $f = 10$ Hz for Figures 2 and 4 in the main text.

S2. Volumetric specific heat capacity measurement

An additional merit of our LIT-based method is that the volumetric specific heat capacity ρ_p of the target materials can be estimated at the same time through the relation $\rho_p = \kappa/D$. Figure S3(a) shows the f dependence of ρ_p of the target materials. In a similar manner to the other parameters, the estimated ρ_p values for $f > 5$ Hz are consistent with the values obtained by the conventional measurement methods. This result indicates that the LIT-based method is also capable of simultaneous non-contact measurements of ρ_p for many materials. Furthermore, the LIT-based method allows us to measure the H dependence of ρ_p [Figure S3(b)]. Unlike the other transport coefficients, the ρ_p values for the materials used in this study show no clear H dependence.

References

- [1] Straube H, Breitenstein O. Estimation of heat loss in thermal wave experiments. J Appl Phys. 2011;109:064515.
- [2] Gałazka K, Populoh S, Xie W, et al. Radiative heat losses in thermal conductivity measurements: a correction for linear temperature gradients. Measurement. 2016;90:187–191.
- [3] Dames C. Measuring the thermal conductivity of thin films: 3 omega and related electrothermal methods. Annu Rev Heat Transf. 2013;16:7–49.
- [4] Çengel YA. Heat transfer: a practical approach. 2nd Edition. McGraw-Hill, Boston; 2003.

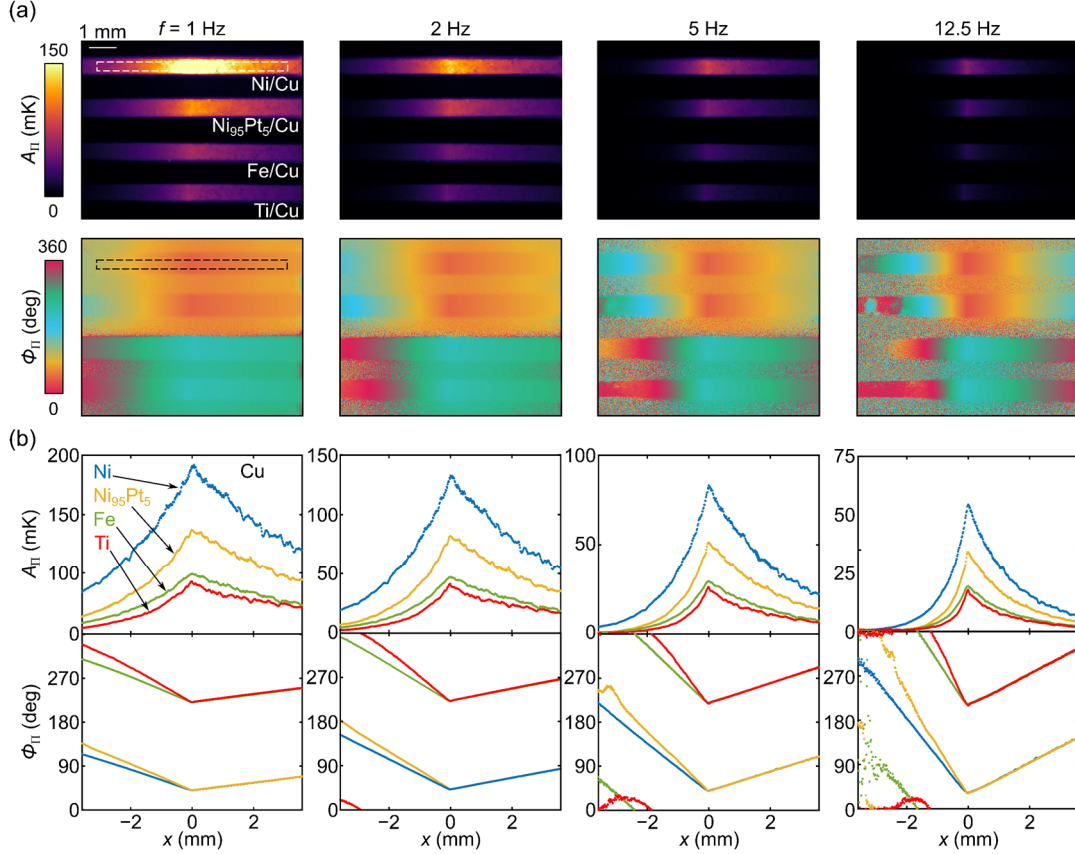


Figure S1. (a) A_{Π} and ϕ_{Π} images and (b) corresponding line profiles for the Ni/Cu, Ni₉₅Pt₅/Cu, Fe/Cu, and Ti/Cu samples for various values of f at $J_c = 1$ A and $\mu_0 H = 0$ mT. The signals shown in this figure are attributed to the Peltier effect at the junctions. The line profiles were obtained by taking the average of the raw profiles over the center areas (dashed rectangles) of the samples.

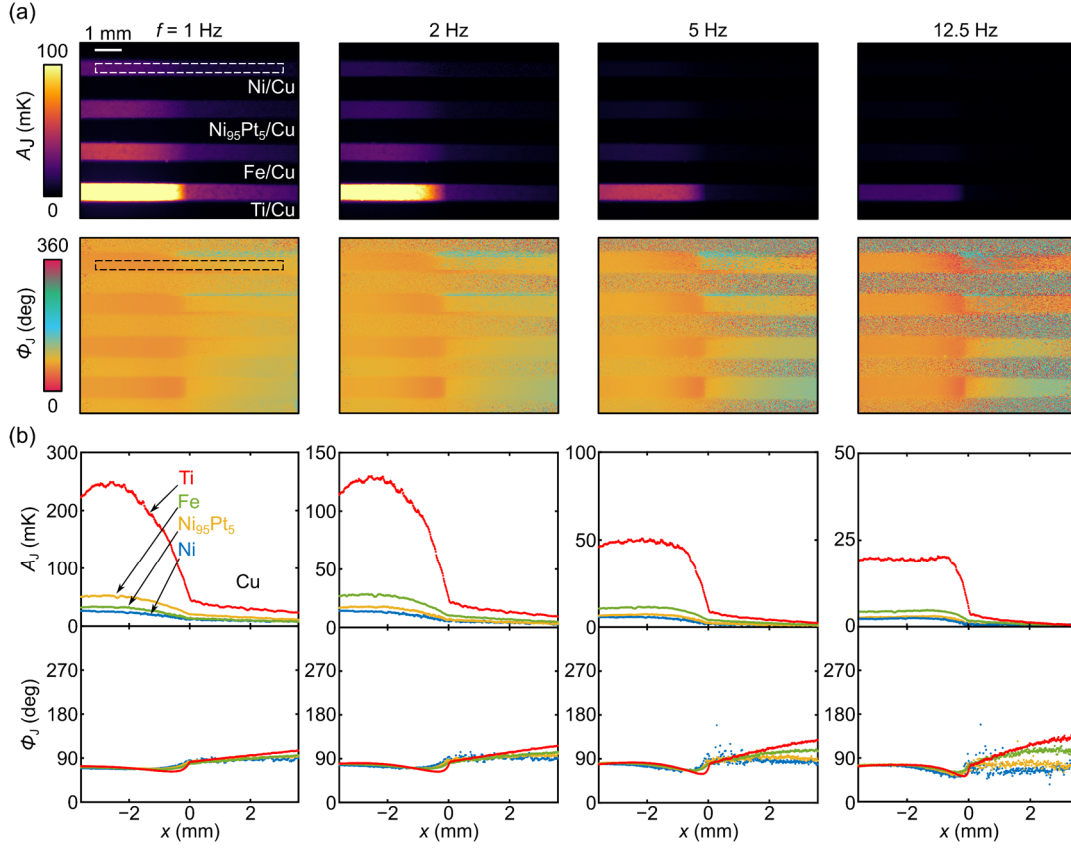


Figure S2. (a) A_J and ϕ_J images and (b) corresponding line profiles for the Ni/Cu, Ni₉₅Pt₅/Cu, Fe/Cu, and Ti/Cu samples for various values of f at $J_c = 1$ A and $\mu_0 H = 0$ mT. The signals shown in this figure are attributed to the Joule heating in the bulk of the materials.

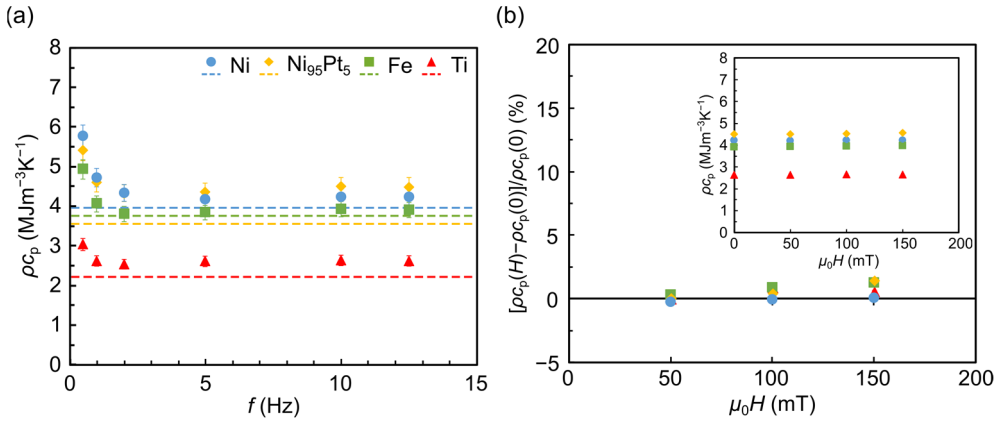


Figure S3. (a) f dependence of ρ_p for the Ni (blue circle), Ni₉₅Pt₅ (yellow diamond), Fe (green square), and Ti (red triangle) samples, estimated from the LIT images at $\mu_0 H = 0$ mT. The dashed lines represent the values estimated from the specific heat capacity measured by the differential scanning calorimetry and density measured by the Archimedes method. (b) H dependence of $[\rho_p(H) - \rho_p(0)]/\rho_p(0)$, estimated from the LIT images at $f = 10$ Hz. $\rho_p(0)$ refers to the volumetric specific heat capacity at $\mu_0 H = 0$ mT. The inset to (b) shows the H dependence of ρ_p .